Available online at www.sciencedirect.com

ScienceDirect

Geochimica et Cosmochimica Acta 318 (2022) 247–262

Geochimica et Cosmochimica Acta

www.elsevier.com/locate/gca

Mechanisms and kinetics of citrate-promoted dissolution of a uranyl phosphate mineral

Brennan O. Ferguson [a,b], Lawrence C. Murdoch [a,b], Michael Trumm [c], Fengjiao Liu [d], Apparao M. Rao [d], Brian A. Powell [a,b,e,*]

[a] Department of Environmental Engineering and Earth Sciences, Clemson University, Anderson, SC 29625, United States
[b] Center for Nuclear Environmental Engineering and Earth Sciences and Radioactive Waste Management, Clemson University, Anderson, SC 29625, United States
[c] Karlsruher Institut für Technologie, Institut für Nukleare Entsorgung, 76021 Karlsruhe, Germany
[d] Department of Physics and Astronomy, Clemson Nanomaterials Institute, Clemson University, Clemson 29634-0978, United States
[e] Department of Chemistry, Clemson University, Anderson, SC 29625, United States

Received 13 May 2021; accepted in revised form 22 November 2021; available online 27 November 2021

Abstract

The formation of uranyl phosphate precipitates is a remediation strategy to limit the mobility of uranium in contaminated soils. However, exposure to organic ligands, like the plant exudate citrate, can remobilize the uranium. The purpose of this study is to provide a more thorough comprehension of citrate-promoted dissolution of a uranyl phosphate mineral, chernikovite [$(H_3O)(UO_2)(PO_4)\cdot 3H_2O$], by determining the extent of uranium release from chernikovite at a wide range of citrate concentrations. We have quantified the kinetics of dissolution and proposed potential mechanisms of chernikovite dissolution to gain a better understanding of the fate of uranyl phosphate precipitates in the environment. Batch dissolution and continuously stirred tank reactor (CSTR) experiments indicate that increasing citrate concentrations from 0.1 mM to 50 mM increases the concentration of dissolved uranium. However, at citrate concentrations of 10 mM and greater, the effectiveness of the ligand to enhance the dissolution decreases. Density functional theory modeling and Raman spectroscopy indicate a strong interaction between citrate and the uranyl ions at the surface of the uranyl phosphate. The interaction between citrate and uranyl suggests the formation of an alteration layer of uranyl-citrate surface complexes, which could impede uranium release at citrate concentrations of 10 mM or higher. Together, these results indicate that the citrate-promoted dissolution of chernikovite is a fast reaction that is hindered by a combination of surface saturation and a secondary-phase precipitation reaction at higher concentrations of citrate and reaction times greater than or equal to 72 min based on the hydraulic residence time of CSTR experiments. These findings improve our understanding of the stability of uranyl phosphate for use in sequestration of uranium groundwater plumes at contaminated sites.
© 2021 Elsevier Ltd. All rights reserved.

Keywords: Chernikovite; Solubility; Dissolution kinetics; Phosphate; Citrate; Uranium; Continuously stirred tank reactor; CSTR

1. INTRODUCTION

Although uranium is a naturally occurring element, the development of nuclear technology has caused extensive uranium contamination around the world predominantly from mining and milling and nuclear energy and weapons production. In the United States, uranium is present above

* Corresponding author at: Department of Environmental Engineering and Earth Sciences, Clemson University, Anderson, SC 29625, United States.
E-mail address: bpowell@clemson.edu (B.A. Powell).

https://doi.org/10.1016/j.gca.2021.11.023
0016-7037/© 2021 Elsevier Ltd. All rights reserved.

action levels in the soil and groundwater at over 120 sites in 36 states and is the most common radionuclide in soils at Department of Energy facilities (Riley et al., 1992; Palmisano and Hazen, 2003; Wellman et al., 2006; Mehta et al., 2015). The release of uranium and potential intrusion into groundwater and surface water poses a significant threat to both the environment and human health not only because the radioactive nature of the element makes it a carcinogenic but also due to the metal's toxic effect on microorganisms, plants, and animals (Craft et al., 2004; Gao et al., 2019). Therefore, uranium contamination must be addressed for the protection of human and environmental health.

The environmental chemistry and geology of anthropogenic uranium contamination sites vary greatly. For example, in the United States, uranium contamination from legacy waste is present in the arid desert of Hanford, Washington with groundwater high in carbonate species and a basic pH, but it is also present in the wetlands of Savannah River Site, South Carolina that has acidic groundwater at nearly pH 4 (Bostick et al., 2002). The large variation in geochemistry at uranium contaminated sites complicates remediation efforts because the mobility of uranium changes with soil characteristics, reduction/oxidation conditions, pH, and the presence of organic matter. Therefore, various geochemical environments must be studied in order to determine possible remediation strategies under site-specific geochemical conditions.

Uranium can exist in oxidation states III – VI. However, in environmentally relevant conditions, uranium primarily exists as U(IV) under reducing conditions and U(VI) in oxidizing conditions. U(IV) is predominantly immobile, often forming a sparsely soluble UO_{2+x} solid (uraninite), while U(VI) has the potential to be highly mobile in the form of the soluble uranyl ion, UO_2^{+2} (Grenthe et al., 2011). Potential uranium remediation strategies for uranium contamination aim to reduce mobile U(VI) uranyl ion through biotic or abiotic means in order to form uraninite or other immobile U(IV) phases. However, exposure to oxygen can remobilize the U(IV), up to 88% of the uranium precipitate, and increase the dissolution rate of uraninite by an order of magnitude (Sani et al., 2005; Liu et al., 2005; Moon et al., 2007; Wu et al., 2007; Ulrich et al., 2009; Grenthe et al., 2011). To avoid remobilization in an oxidizing environment, an alternative remediation method immobilizes the uranyl ion by precipitating uranyl phosphate minerals (Fuller et al., 2002; Luo and Gu, 2011; Fanizza et al., 2013; Mehta et al., 2014; Perdrial et al., 2018). Uranyl phosphate minerals are stable under oxidizing conditions and can precipitate faster and are less soluble than other non-phosphate U(VI) minerals (Gorman-Lewis et al., 2008; Wang et al., 2017).

Uranyl phosphates exhibit extremely low solubility under circumneutral pH with log K_{sp} −12.17 for synthetic chernikovite to −49.36 for uranyl orthophosphate $[(UO_2)_3(PO_4)_2{\cdot}4H_2O]$ (Gorman-Lewis et al., 2008). The K_{sp} refers to the solubility product constant or the equilibrium constant between a solid and its dissolved ions. Therefore, the higher the K_{sp} value is the more soluble the solid. In comparison to uranyl phosphates, uranyl oxide hydrates, often the first phase formed when uranium is oxidized in uranium deposits, are significantly more soluble with reported log K_{sp} values ranging from 5.52 to 43.70. At some locations with a high uranium presence, like the Fernald site in Ohio and the DOE-K25 site at Oak Ridge, Tennessee, the uranyl phosphate, autunite, governs the release of uranium (Buck et al., 1996; Murakami et al., 1997).

This research focuses on the uranyl phosphate chernikovite which is composed of sheets of polyhedra consisting of uranyl square bipyramids and phosphate tetrahedra (Burns, 2005). The interlayer between two sheets consists of water molecules and hydronium ions. Like all autunite group minerals, chernikovite forms at pH < 8 in the presence of oxidized uranium and phosphate. Previously published studies have also synthesized chernikovite, when mixing soluble uranyl nitrate and sodium phosphate salt solutions under rapid mixing conditions, even though other minerals like uranyl orthophosphate, sodium-autunite $(Na_2[(UO_2)(PO_4)]_2{\cdot}3H_2O)$, and autunite $(Ca[(UO_2)(PO_4)]_2{\cdot}4H_2O)$ were more thermodynamically favorable (Giammar, 2001; Fanizza et al., 2013; Mehta et al., 2014). Thus, it appears that while chernikovite may be thermodynamically unfavorable compared to other uranyl phosphate phases, chernikovite may be kinetically favorable during rapid precipitation of uranyl phosphates from soluble salts. Therefore, in many natural conditions, chernikovite could be the initial uranyl phosphate phase, but with time and exposure, chernikovite would convert to more common uranyl phosphate phases, like autunite.

The mineral chernikovite has several reported solubility constants in literature with synthetic chernikovite having log K_{sp} values ranging from −12.17 to −13.17 (Veselý et al., 1965; Gorman-Lewis et al., 2009) while natural chernikovite has a reported log K_{sp} value of −22.73 and is therefore less soluble (Van Haverbeke, 1996). The difference in solubility between synthetic and natural chernikovite could be due to a difference in particle size or crystallinity since a more ordered (crystalline) mineral is less soluble. The substitution of the hydronium ion in the interlayer for a sodium cation (Na-autunite) or calcium cation (autunite) results in less soluble uranyl phosphate minerals with log K_{sp} values of −47.4 and −48.4 respectively (Gorman-Lewis et al., 2008). This large range of K_{sp} values in chernikovite and similar uranyl phosphates leads to highly variable, solubility-controlled uranium concentrations and sensitivity to the precipitated uranyl phosphate phase. In this work, it is hypothesized that while the initial chernikovite dissolves, another uranyl phosphate forms as a secondary-phase precipitate, less soluble than chernikovite. This possible precipitation of a secondary-phase uranyl phosphate mineral could have a large impact on aqueous uranium concentrations and lead to a changing equilibrium point of the system during dissolution.

In addition to the characteristics of the solid phase of the uranyl phosphate mineral, other environmental factors, like pH and dissolved organic matter, can affect the release of uranium by dissolution (Sowder et al., 2001; Gorman-Lewis et al., 2008; Luo and Gu, 2011; Gudavalli et al., 2013). Organic ligands have been found on DOE sites as co-contaminants with radionuclides and are also produced by microorganisms and plant roots from metabolic

processes (Riley et al., 1992). Like other metals, uranium can form strong complexes with organic ligands, which can increase the mobility of uranium in the environment. The presence of organic ligands in solution can increase the solubility of a mineral by complexing with the aqueous metal cation, forming a more soluble species, and therefore driving the dissolution reaction forward to release more metal cations in solution (Banfield et al., 1999; Welch et al., 1999; Cervini-Silva, 2005). The organic ligand citrate is an effective complexing agent for several metals and is also a common root exudate produced by plant roots to assist in the uptake of nutrients from the soil. Because of these characteristics, citrate was the organic ligand chosen to study the ligand-promoted dissolution of chernikovite.

Previous work has emphasized the complex relationship between minerals, ligands, and plants. Edayilam et al. (2018) examined the effect of different phosphate sources with varying solubilities on the release of metabolites from plant roots. The conclusions of the study suggest that the presence of sparsely soluble and therefore lower bioavailable phosphate solids, like $FePO_4$ and $Ca_3(PO_4)_2$, increases the release of organic acids including citrate from plant roots when compared to systems with highly soluble phosphate sources like KH_2PO_4 or no phosphate sources at all. In particular, the organic ligand citrate reached concentrations of 1 mM pore water in systems with the less soluble phosphate sources. Citrate has also been linked to increased uranium uptake in plants (Ebbs et al., 1998; Huang et al., 1998; Francis and Dodge, 1998; Shahandeh and Hossner, 2002). These studies demonstrate the importance of understanding organic ligand/uranyl phosphate systems because phosphate minerals can affect the release of organic ligands from plant roots which can in turn affect the mobility of uranium.

Previous studies have focused on autunite or chernikovite dissolution at neutral to basic pH, with EDTA, citrate, bicarbonate and TRIS [tris (hydroxymethyl)aminomethane] (Sowder et al., 2001; Wellman et al., 2006; Luo and Gu, 2011; Gudavalli et al., 2013, 2018; Reinoso-Maset et al., 2020). The findings presented in some of these works suggest that uranium dissolution increases with increasing ligand concentrations, but in other studies, there is very little change in uranium dissolution despite increasing ligand concentrations. Using single-pass flow-through experiments to examine a bicarbonate and autunite system, Gudavalli et al. (2013) increased the bicarbonate concentrations of the influent by a factor of ten from 0.3 mM to 3 mM and observed an increase in the dissolution rate of autunite by a factor of 18 at neutral pH. However, for the same system when the bicarbonate concentration of the influent solution was increased from 25 to 100 mM (only a factor of four increase in bicarbonate concentrations) the autunite dissolution rate increases by a factor of 30 with dissolution rate values two orders of magnitude greater than the rates reported with 3 mM bicarbonate influent solution (Gudavalli et al., 2018). Gudavalli et al. (2013) also proposed a two-step dissolution mechanism consisting of the formation of uranyl-carbonate surface complexes followed by the release of the uranyl-carbonate complexes into the solution. Similarly, Reinoso-Maset et al. (2020) reported an increase in dissolved uranium from K-ankoleite, Na-autunite, and Ca-autunite sources with increasing carbonate concentration in the influent of flow-through column experiments. In experiments with 0.2 mM carbonate solution and a pH of 7 in the influent, Reinoso-Maset et al. (2020) observed dissolved uranium concentrations reaching 0.4 μM for Ca-autunite source and 0.2 μM for K-ankoleite and Na-autunite. When the carbonate influent solution was increased by an order of magnitude with a pH of 8, the dissolved uranium concentrations increased to 20 μM for Ca-autunite sources and 30 μM for K-ankoleite and Na-autunite. In a single-pass flow-through study of autunite dissolution in TRIS buffer (used as an analogue for more complex natural organic matter) at neutral to basic pH, Wellman et al. (2006) reported an increase in the dissolution rate by a factor of 35 for a five-fold increase in TRIS concentration from 0.01 M to 0.05 M.

Using batch experiments, Luo and Gu (2011) also observed an increase in the dissolution of an unknown uranyl phosphate phase from contaminated sediments with increasing ligand concentration in solution at pH 6.5, but only when EDTA was used as the facilitating ligand and not citrate. In experiments with 0.4 mM EDTA in solution, dissolved uranium from uranyl phosphate sources was not detected, but in experiments where EDTA was increased by a factor of two to 0.8 mM the dissolved uranium concentrations from uranyl phosphate sources increase to 1.8 μM. However, in experiments with citrate, the dissolved uranium concentration from the uranyl phosphate remained relatively constant at 1.8 μM in 0.7 mM citrate solution and 2.1 μM in 1.4 mM citrate solution. Conversely, the results from Sowder et al. (2001) did not show an increase in dissolved chernikovite in batch experiments at pH 7.2 as EDTA concentration increased since the system with 1 mM EDTA solution results in 5% of the uranium source dissolved, but when the EDTA concentration increased by two orders of magnitude to 100 mM, negligible chernikovite dissolution was observed. However, in experiments with bicarbonate at pH 8.3, less than 5% of the uranyl phosphate dissolved in the 1 mM bicarbonate solution while the uranyl phosphate dissolved completely in the 100 mM bicarbonate solution. The findings in these studies generate questions regarding the consistency of ligands, particularly organic, to facilitate dissolution of uranyl phosphate and the factors that could impact the rate and extent of ligand promoted dissolutions.

The conflicting results from previous studies regarding the effect of increasing ligand concentrations on the dissolution of uranyl phosphate and the extent of any observed increase in uranium dissolution highlight a gap in the understanding of ligand-promoted dissolution, especially in acidic conditions since previous work has focused on neutral to basic pH systems. Dissolution kinetics of a uranium source in the presence of organic matter in particular are important to plant-uptake studies, field-scale studies, and predicting the overall mobility of uranium release from uranyl phosphate in the environment. The overall objective of this investigation is to characterize the effect of citrate on the dissolution of chernikovite to better understand

uranium bioremediation/phytoremediation efforts in an acidic system. Besides serving as an analogue for acidic environments, like the wetlands of the Savannah River Site, studying organic ligand-promoted dissolution at an acidic pH isolates the effect of the organic ligand on the dissolution reaction without the interference from carbonate species that occurs at basic to neutral pHs. More generally, these data will serve to better understand the complexity of multicomponent tertiary (uranyl component, phosphate component, and organic component) dissolution systems. This led to three sub-objectives: (1) create a dataset describing chernikovite dissolution at different citrate concentrations, (2) formulate a conceptual model describing mechanisms for citrate-promoted dissolution of uranyl phosphate, (3) determine rate constants for the dissolution reaction.

2. MATERIALS AND METHODS

This study used both batch and continuously stirred tank reactor (CSTR) dissolution tests to evaluate the effects of citrate on the dissolution of chernikovite. Batch dissolution and citrate-sorption studies determined the effect of increasing citrate concentration on uranyl phosphate dissolution while also indicating potential mechanisms for the citrate-promoted dissolution reaction. Chernikovite was dissolved in a CSTR with varying flow rates and citrate concentrations to quantify the kinetics of citrate-promoted dissolution of uranyl phosphate. A CSTR experiment is an ideal method for kinetic studies because the setup maintains a dilute solution that is far from equilibrium to drive the reaction forward by removing the reaction products that could influence the reaction rate or alter the solubility of the starting mineral (Seyfried et al., 1989; Sparks, 1989; Bar-Tal et al., 1990; McGrail et al., 1997; Ulrich et al., 2009). Because CSTRs are assumed to be thoroughly mixed systems, this method minimizes the effects of transport phenomena, like dispersion, that must be considered in single-pass flow-through experiments and allows for greater control of the extent of reactions (i.e., reaction rates) based on precise control of the hydraulic residence time.

2.1. Solutions

Citrate solutions with concentrations ranging from 0.1 mM to 50 mM were prepared using sodium citrate dihydrate ($Na_3C_6H_5O_7{\cdot}2H_2O$) in deionized water from a PURELAB flex water system. This range of citrate concentrations was chosen to encompass the root exudate concentrations reported in Edayilam et al. (2018). In experiments without citrate, a 10 mM sodium chloride solution was used to provide background electrolytes. All solutions were pH adjusted to 4 using 1 M HCl. The citric acid labeled with ^{14}C used in the citrate sorption kinetic study was obtained from American Radiolabled Chemicals Inc.

2.2. Synthesis of chernikovite

The chernikovite was synthesized by mixing 20 mL of 0.3 M uranyl nitrate hexahydrate [$UO_2(NO_3)_2{\cdot}6H_2O$] from International Bio-Analytical Industries Inc. (ACS 98.0–102%) and 20 mL of 0.31 M sodium phosphate dibasic heptahydrate [$Na_2HPO_4{\cdot}7H_2O$] prepared in deionized water (Fanizza et al., 2013). The mixture was placed on a tube rotator and allowed to react for 24 h. The mixture was then centrifuged, and 85% of the supernatant was removed and replaced with fresh deionized water. After resuspending the solid, this rinsing cycle was repeated three times to ensure the removal of free ions from the precipitate. After rinsing, the precipitate was placed in a desiccator to dry. Precipitate was characterized as chernikovite using x-ray diffraction (XRD) and electron dispersive spectroscopy (EDS) (Fig. S1). The surface area was determined as 2.10 ± 0.26 m^2/g using BET techniques.

2.3. Batch dissolution experiments

For batch dissolution experiments, 12 samples were prepared with 30 mg of chernikovite in 12 mL of solution. The synthesized chernikovite was washed an additional seven rinse cycles in 10 mM NaCl solution using the same centrifuging, supernatant removal, and resuspension of solid procedure that was described in the chernikovite synthesis section. These rinses simulated the washing step in the flow experiments, which flushed out any excess aqueous uranium and provided a more uniform solid. Each sample solution had a different citrate concentration (0, 0.1 mM, 0.5 mM, 1 mM, 5 mM, 10 mM, 15 mM, 20 mM, 25 mM, 30 mM, 40 mM, and 50 mM), and all solutions were pH adjusted to 4. Samples were placed on a tube rotator for 12 h before 2 mL aliquots were removed and filtered using a 0.2 μm polypropylene syringe filter. A portion of the filtered solution was diluted by a factor of 1000 in 2% HNO_3 by weight for aqueous uranium concentration analysis by a Thermo Scientific X series 2 inductively coupled plasma-mass spectrometer (ICP-MS). After collecting the aliquots, the samples were returned to the tube rotator and allowed to mix for one week after which the sampling was repeated. The pH of the samples was measured at both sampling times. All experiments were performed under atmospheric conditions. Uranium speciation and concentrations of the batch systems were simulated using the geochemical modeling software Visual MINTEQ v.3.1 (maintained by J. Gustafsson at KTH, Sweden) and the minteq database. To verify the MINTEQ results, some simulations were also performed using the United States Geological Survey program PHREEQC.

2.4. Citrate sorption to chernikovite experiment

As in the batch dissolution experiments, the synthesized chernikovite was washed an additional seven rinse cycles in 10 mM NaCl solution. The concentration of solid chernikovite used was 2.5 mg/mL in 45 mL of 0.1 mM citrate spiked with 25 μL of ^{14}C-citrate to have a 41.7 Bq/mL activity concentration (equivalent to 0.001 mM of citrate). The mass of ^{14}C-citrate added was insignificant to the total concentration of citrate in the sample. The sample was resuspended, and then 2 mL of solution was immediately removed and filtered using 0.2 μm polypropylene syringe filter. The

sample was placed on a tube rotator and was sampled at 15 min, 30 min, 1 h, 3 h, 8 h, and 24 h. A 0.5 mL aliquot of the filtered samples from each sampling time was mixed with 5 mL of HiSafe 3 (PerkinElmer) liquid scintillation cocktail and counted using a Tri-Carb Liquid Scintillation Analyzer to measure ^{14}C and subsequently the aqueous citrate concentration. The aqueous citrate concentration was determined by multiplying the fraction of ^{14}C remaining in solution by the total citrate concentration in solution (e.g., isotope dilution). The uranium concentration was determined by ICP-MS as described in Section 2.3. A control without the uranyl phosphate solid was also included to account for any citrate sorption to the vial.

2.5. Continuously stirred tank reactor experiments

The continuously stirred tank reactor (CSTR) was a polytetrafuoroethylene apparatus with a volume of 17.9 mL and a detachable top and bottom (Fig. S2). For each experiment, 100 mg of chernikovite was loaded into the reactor along with a stir bar. A 0.1 μm Omnipore Membrane filter was placed between the bottom piece of the reactor, where the influent entered, and the top piece, where the effluent exited, to prevent chernikovite particles from leaving the reactor in the effluent. Initially, the reactor was filled with a 10 mM NaCl solution at pH 4 by pipetting the solution directly into the hole used for the influent. A peristaltic pump was used to pump the influent solution into the CSTR, and the effluent was collected in approximately 5 mL aliquots using an Eldex fraction collector.

Four experiments were performed with each experiment having a different citrate concentration in the influent solution: no citrate (consisting of 10 mM NaCl solution), 0.1, 1, and 10 mM citrate. Additional NaCl was not added to normalize the ionic strength among the four experiments with different citrate concentrations because based on Visual MINTEQ speciation modeling for this particular system, uranyl-citrate are the dominant complexes (as opposed to sodium-citrate or uranyl-chloride). In order to reach steady state, the chernikovite precipitate inside the reactor was pretreated first with 10 mM NaCl solution and then with citrate solution to produce a more uniform chemical environment, similar to the pretreatment used in Cervini-Silva et al. (2012) and Ulrich et al. (2009) (Table 1). This pretreatment step utilizing citrate was not used for the citrate-free experiments. The pretreatment method was followed by the dissolution experiment where the flow rate was consecutively reduced from 1 mL/min to 0.5 mL/min to 0.25 mL/min after five reactor volumes at each rate. One reactor volume was 17.9 mL leading to hydraulic residence times of 17.9 min at 1 mL/min, 35.8 min at 0.5 mL/min, and 71.6 min at 0.25 mL/min. This resulted in an overall duration of each experiment of approximately 11.7 h (1.7 h at 1 mL/min, 3.3 h at 0.5 mL/min, and 6.7 h at 0.25 mL/min). The pH of the collected effluent was measured, and the uranium concentration was determined by ICP-MS using the same method as described in Section 2.3. Remaining solids from the experiments were completely dissolved in 1 M HNO_3, and the uranium and phosphorous ratio of the solids were determined using a Perkin-Elmer Optima 3100 ICP-OES (inductively coupled plasma-optical emission spectroscopy). The experimental conditions for each citrate concentration tested are provided in Table 2, and all experiments were performed under atmospheric conditions.

Table 1
A description of the pre-treatment method and the dissolution experiment for the CSTR.

Pre-treatment Method		
Influent Solution	Flow rate (mL/min)	Reactor volumes
10 mM NaCl	0.25	10
Citrate solution*	0.25	5
Citrate solution	0.5	5
Citrate solution	1	5
10 mM NaCl	0.25	10
Dissolution Experiment		
Influent Solution	Flow rate (mL/min)	Reactor volumes
Citrate solution	1	5
Citrate solution	0.5	5
Citrate solution	0.25	5

* Citrate solution concentration is consistent throughout a single experiment but could refer to 0.1 mM, 1 mM, or 10 mM citrate concentrations.

2.6. Solid phase characterization

The synthesized chernikovite was analyzed before and after citrate exposure using a variable pressure scanning electron microscope, Hitachi model S-3400. Samples were prepared by suspending solids in DI water and pipetting suspended solution onto carbon tape attached to a standard SEM stub. Additionally, portions of the remaining precipitate after batch and CSTR dissolution experiments were pipetted from a suspended solution onto a glass slide and air dried for analysis by a Cu source Rigaku MiniFlex X-ray diffractometer. For Raman analysis, the samples were prepared in the same manner as they were for the XRD. Raman spectra were collected with a 785 nm excitation laser in a Renishaw inVia Raman microscope (100x objective lens).

2.7. Structure optimization

Possible structures of citrate ions replacing phosphate ions coordinating to U(VI) via either a terminal carboxyl group (end-on) or central carboxyl group (middle) have been optimized for 1:1, 1:2 and 1:4 complexes. Solvent effects were taken into account by saturation with 50 water molecules. Density functional theory (DFT) using the B3-LYP functional was employed (Lee et al., 1988; Becke, 1993). U was described by a small-core pseudo potential ECP60MWB with corresponding basis sets of triple-zeta quality (Küchle et al., 1994). All other atoms were described by the def2-TZVP basis sets as implemented in the TURBOMOLE software package (TURBOMOLE V6.4 2012, a development of University of Karlsruhe and Forschungszentrum Karlsruhe GmbH, 1989–2007, TURBOMOLE GmbH, since 2007; available from

Table 2
Experimental conditions and amount of uranium dissolved for the CSTR experiments.

Citrate Concentration	Ionic Strength of Solution (M)	Initial U (mol)	Total Dissolved U[§] (mol)	% of initial	Dissolved U during Experiment (mol)	% of post-wash*
no citrate	0.0101	1.14×10^{-4}	4.64×10^{-6}	4.06%	–	–
0.1 mM citrate	9.06×10^{-4}	2.28×10^{-4}	2.95×10^{-5}	12.9%	1.12×10^{-5}	5.32%
1.0 mM citrate	0.00807	1.60×10^{-4}	7.34×10^{-5}	45.9%	2.44×10^{-5}	22.0%
10 mM citrate	0.0820	2.28×10^{-4}	8.86×10^{-5}	38.8%	2.77×10^{-5}	16.6%

[§] Refers to total dissolved uranium including both the pretreatment wash and the dissolution experiment.
* Refers to the percentage of uranium dissolved during the experiment out of the uranium remaining after the pretreatment wash.

http://www.turbomole.com). No periodic boundary conditions were applied. After the optimization all geometries were proven to be true minima by vibrational frequency calculation. From the resulting structures, vibrational Raman scattering cross sections were computed from derivatives of the frequency-dependent polarizability tensor with respect to normal modes of vibration:

$$\frac{d\sigma}{d\Omega} = k_\omega\left(c_i\alpha'^2(\omega) + c_a\gamma'^2(\omega)\right) \quad (1)$$

Here, $\alpha'^2(\omega)$ and $\gamma'^2(\omega)$ respectively denote the isotropic and anisotropic part of the differentiated polarizability tensor. The coefficients c_i and c_a depend on the scattering geometry and the polarization of the incident and scattered radiation. Vibronic frequencies ω_v and degeneracies g_v are taken into account in the prefactor.

$$k_\omega = \left(\frac{\hbar}{4\pi\varepsilon_0^2 c^4}\right)\frac{(\omega-\omega_v)^4 g_v}{2\omega_v} \quad (2)$$

where c is speed of light and ε_0 the dielectric constant of vacuum.

2.8. Dissolution Model of CSTR data

This modeling approach assumes a perfectly mixed CSTR system to evaluate changes in uranium effluent concentrations versus time. The rate for the citrate-promoted dissolution of chernikovite was characterized as:

$$\frac{d[U]_{eff}}{dt} = -\frac{Q}{V}[U]_{eff} + k[cit]^n\left(1-\frac{[U]_{eff}}{[U]_{eq}}\right) \quad (3)$$

where $[U]_{eff}$ (mol L^{-1}) is the uranium concentration in the effluent, Q (L s^{-1}) is the flow rate, V (L) is the volume of the reactor, $[U]_{eq}$ is the predicted concentration of dissolved uranium at equilibrium, [cit] is the citrate concentration which remains constants throughout the experiment, and n is the reaction order with respect to citrate. To evaluate experiments with constant citrate concentrations, the overall reaction rate constant, k, was simplified to the pseudo zero-order reaction constant k′ as:

$$k' = k[cit]^n \quad (4)$$

and combined with equation (3) to yield:

$$\frac{d[U]_{eff}}{dt} = -\frac{Q}{V}[U]_{eff} + k'\left(1-\frac{[U]_{eff}}{[U]_{eq}}\right) \quad (5)$$

The uranium effluent concentration, $[U]_{eff}$, from Eq. (5) was fit to the experimental data by adjusting k' using the method of least squares in Excel Solver, and then k' values from each experiment with varying citrate concentrations was used in Eq. (4) to determine the reaction order with respect to citrate (n) and the overall reaction constant (k). A similar approximation assuming steady state conditions was reported by Gudavalli et al. (2013). Preliminary modeling results indicated significant mismatch between the model and data when one value of k' was used for all experiments. This suggests that k' depends on flow rate and citrate concentration, so each experiment was analyzed individually to evaluate this effect. As discussed below in Sections 3.4, 4.2, and 4.5, the observed effluent uranium concentrations in these data are more dependent on the citrate concentration than the change in chernikovite mass in the system due to the large initial mass of uranyl phosphate. To verify the infinite solid assumption, a model was tested that accounted for decreasing solid phase concentration as done by Ulrich et al. (2008), but there was no overall improvement of the reaction rate constants or model fit. Therefore, the models presented are in terms of uranium concentrations and citrate concentrations rather than mineral surface area normalized concentrations.

In addition to the simple model from Eq. (5) several alternate models were evaluated including:

- shrinking core, which considers mass transfer of uranium from spherical grain dissolution accounting for a decrease in grain radius with dissolution
- stepwise reactions considering citrate and uranium saturation of the mineral surface
- secondary-phase precipitation of a less soluble form

These models had varying success in approximating the observed uranium aqueous concentrations, and none were significantly better than the simple analysis given in Eqn. (5). As discussed below in Sections 3.4, 4.2, and 4.5, the simple model presented in Eq. (5) approximates the data but results in rate constants that appear to slightly change with reactor flow rate. This work proposes that these changes in the determined rate constants are due to underlying reactions within the conceptual models listed above, primarily secondary-phase precipitation. While the other reactions considered in the conceptual models above likely have some influence on the system, in keeping with the

principle of parsimony, we adopted the simple, but effective model given by Eq. (5).

3. RESULTS

The results include data from dissolution experiments conducted using batch and CSTR techniques, along with theoretical calculations that explain and interpret those data. Chemical analyses using Raman spectroscopy and XRD are presented to evaluate surface effects, including mineral precipitation, alteration, and citrate saturation, that affect interpretation of the batch and CSTR dissolution data.

3.1. Batch dissolution experiments

The batch dissolution experiments (Section 2.3) examined the effect of increasing citrate presence on the dissolution of chernikovite with dissolved uranium concentrations measured at 12 h and one week. Without the addition of citrate, the dissolved uranium concentration was 11.6 μM at 12 h and 8.05 μM at a week (Fig. 1), in agreement with the concentrations reported in previous studies (Gorman-Lewis et al., 2009; Mehta et al., 2014). The dissolution of chernikovite generally increased with increasing citrate concentrations. The increase in citrate concentration by a factor of five, from 0.1 mM to 0.5 mM, resulted in an increase in the dissolved uranium concentrations by a factor of 3.2. However, another increase by a factor of five but at a higher concentration, from 10 mM to 50 mM citrate, only increased the dissolved uranium concentrations by a factor of 1.2. There were no discernable changes in dissolved uranium concentrations between 12 h and one week except for the slight increase observed at one week for the two highest citrate concentrations tested. The total dissolved uranium in this experiment for all citrate concentrations was less than 15% of the total uranium in the sample, so solid uranyl phosphate remained in the experiment for further dissolution.

The simulated dissolved uranium concentrations generated by the geochemical modeling software follow a similar trend to the experimental data, but they under-predict the observed concentrations from the batch experiments (Fig. 1). The model also predicts the formation of the less soluble uranyl orthophosphate as a secondary-phase in systems with less than 10 mM of citrate added and Na-autunite mineral in systems with citrate concentrations greater than 1 mM.

3.2. Citrate sorption to chernikovite

The concentration of sorbed citrate on the chernikovite surface was evaluated over time to provide insight into the reaction mechanism for the citrate-promoted dissolution of chernikovite. Less than one minute after citrate was added, 41 μM of uranium was released, and 1.1 μM of citrate was sorbed to the mineral. Citrate continued to remain almost entirely in the aqueous phase as the uranium concentration peaked at 52.5 μM at 30 min (Fig. 2). The uranium concentration then steadily decreased to 43.9 μM while the sorbed citrate increased after 3 h reaching 11.1 μM sorbed by 24 h.

3.3. Solid phase characterization

3.3.1. Elemental Analysis

The elemental analysis of the uranyl phosphate remaining after exposure to 0.1, 1.0, and 10 mM citrate from the CSTR experiments maintained a 1:1 uranium to phosphorus ratio.

3.3.2. XRD

Comparison of the XRD patterns from the synthesized chernikovite starting material and the uranyl phosphate post-experiment show no distinguishable changes in peak position after citrate exposure (Fig. S1). A peak near 6.95 Å as well as smaller additional peaks throughout the diffraction pattern occurred in all the diffraction patterns from the solid remaining after citrate exposure. These peaks were not in the starting material pattern or the chernikovite reference but match the reference pattern of a sodium citrate. Therefore, it is likely that a sodium citrate salt formed as the XRD samples were drying. The samples were not washed during the preparation because the process could remove alteration layers that formed on the surface.

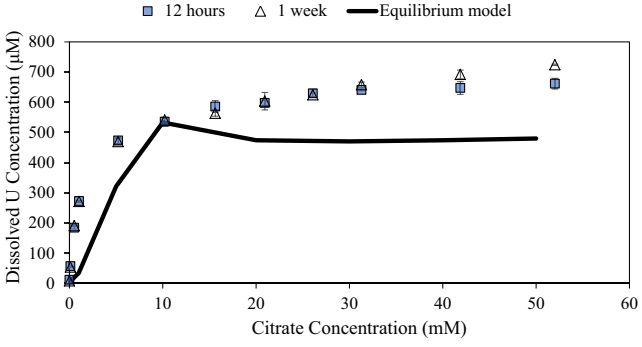


Fig. 1. Dissolution of chernikovite in batch experiments sampled at 12 h and one week with 12 different concentrations of citrate at pH 4. Instrumental error bars are plotted but most are smaller than marker size. The black line represents the dissolved uranium concentrations predicted at equilibrium using Visual MINTEQ.

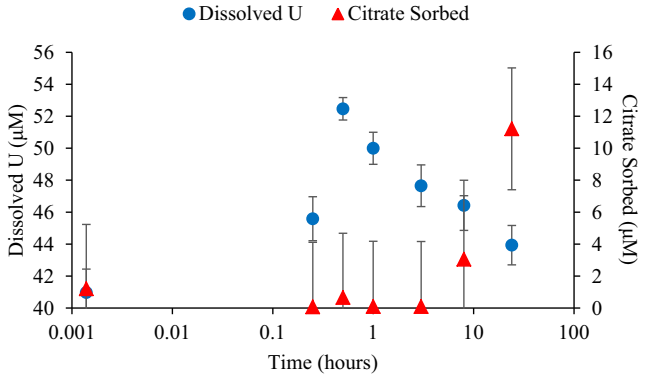


Fig. 2. The dissolved uranium concentrations and sorbed citrate concentrations over 24 h in a 0.1 mM citrate system. The error bars are the standard deviation of the instrument analysis.

3.3.3. SEM/EDS

Images from the SEM also show no observable changes between the chernikovite starting material and the remaining solid after citrate exposure (Fig. S3). The images from chernikovite both pre- and post-citrate exposure depict well-defined, homogenous particles about 1 μm in diameter. However, the EDS analysis revealed a change in the molar ratio composition. The starting material had a molar Na:P:U ratio of 0.27:0.80:1.0 which is consistent with a predominantly chernikovite solid and the possible presence of some Na-autunite. The molar Na:P:U ratio for the uranyl phosphate exposed to 10 mM citrate was 0.91:0.96:1.0 which is the molar ratio of a predominantly Na-autunite solid.

3.3.4. Raman

Raman analysis reveals a change in the Raman spectra of chernikovite after exposure to citrate. The Raman spectrum of the synthesized chernikovite starting material with no citrate has two peaks in the region corresponding to the symmetric stretching of PO_4 with the greater peak at 1033 cm^{-1} and the lesser peak at 981 cm^{-1} (Fig. 3a) which is consistent with previous spectra of chernikovite reported in the literature (Clavier et al., 2016). The most prominent peak in the measured Raman spectrum occurs at 865 cm^{-1} and corresponds to the symmetric stretching of UO_2. The uranyl phosphate remaining after the 0.1 mM citrate CSTR experiment exhibited a Raman spectrum that is similar to

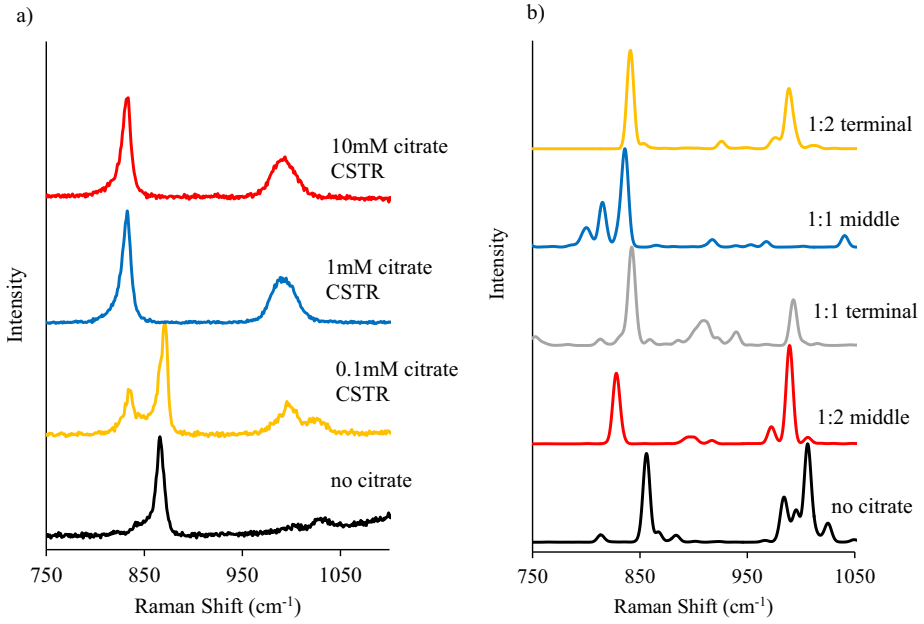


Fig. 3. Raman spectra for (a) experimental solids, including the initial uranyl phosphate starting material before exposure to citrate (no citrate), the solid remaining after the CSTR dissolution experiments with three different citrate concentrations, and (b) predicted Raman spectra based on density functional theory calculations for a uranyl phosphate system with no citrate (no citrate), a system with a uranyl to citrate ratio of 1:2 where the middle carboxyl groups complex with the uranyl ion (1:2 middle), a system with a 1:1 uranyl to citrate ratio where a terminal carboxyl group complexes with the uranyl ion (1:1 terminal), a system with a 1:1 uranyl to citrate ratio where the middle carboxyl group complexes with the uranyl ion (1:1 middle), and a system with a 1:2 uranyl to citrate ratio where terminal carboxyl groups complex with the uranyl ion (1:2 terminal).

Table 3
Computed bond distances in angstrom for the optimized structures of citrate ions coordinating to U(VI) via either a citrate terminal carboxyl group (end-on) or the citrate central carboxyl group (middle) for 1:1 and 1:2 uranium to citrate ratio complexes.

		UO_2 [Å]	UO phosphate [Å]	UO citrate [Å]
phosphate		1.83	2.28	–
end-on	1:1	1.81	2.25	2.38
	1:2	1.79	2.28	2.34
middle	1:1	1.83	2.25	2.33
	1:2	1.83	2.24	2.31

the starting material, with the presence of an additional weak peak at 834 cm^{-1}. In the PO_4 stretching region, the spectrum from the 0.1 mM citrate experiment retained the two peaks, though the greater peak was at 996 cm^{-1} while the lesser peak was at 1026 cm^{-1}. The Raman spectra for the precipitate remaining after the 1 mM and 10 mM citrate CSTR experiments have only a single broad peak in the PO_4 stretching region at 989 cm^{-1} and 994 cm^{-1} respectively. A single UO_2 stretching peak is present in these spectra at 833 cm^{-1} for the 1 mM citrate experiment and 834 cm^{-1} for the 10 mM citrate experiment.

Several theoretical Raman spectra were computed by varying the uranyl to citrate molar ratio from 1:1 to 1:2 and altering the carboxyl group that complexed to the uranyl ion from the terminal carboxyl group to the middle carboxyl group of the citrate molecule. The optimized structures show only small influence of the ligand on the uranyl bond (Table 3.). Uranium-ligand bond lengths are slightly longer (0.07–0.10 Å) for citrate compared to phosphate. In all cases, the citrate ion coordinates via a mono-dentate coordination mode to uranium within the equatorial plane (Fig. S4). Theoretical Raman spectra were obtained by adding a gaussian line broadening to the computed positions. The determined theoretical spectra corroborate the spectra from the experimental systems (Fig. 3b). The spectrum generated from the theoretical system without citrate also resembles the spectra of chernikovite in literature (Driscoll et al., 2014; Clavier et al., 2016). Several peaks are present in the PO_4 stretching region from 984 cm^{-1} to 1027 cm^{-1} with the greatest at 1006 cm^{-1}, and a prominent peak is present in the UO_2 stretching region at 856 cm^{-1} (Fig. 3b). The citrate system with a 1:2 uranyl to citrate molecule ratio with the middle carboxyl groups coordinating with the uranyl ion for both citrate molecules (1:2 middle) produced the Raman spectrum most similar to the spectra from the two higher citrate concentration experiments. The theoretical spectrum of the 1:2 middle system has fewer peaks in PO_4 stretching region with the largest peak at 989 cm^{-1} and a smaller UO_2 peak downshifted to 828 cm^{-1}. The other theoretical combinations for the systems with citrate yield Raman spectra where the UO_2 stretching peak has less of a downshift with peaks at 841 cm^{-1} for 1:2 end-on system and 845 cm^{-1} for 1:1 end-on system. Although the spectrum of the 1:1 middle system has a prominent peak at 836 cm^{-1}, no noticeable peaks are present in the PO_4 stretching region and additional peaks are present at smaller Raman shifts that are not observed in the experimental Raman spectra. Determined energies and structures for the 1:4 end-on and middle complexes were unfavorable and are hence not considered for further investigation.

3.4. Continuously stirred tank reactor experiments

Preliminary experiments indicated that a pretreatment step (Table 1) where the chernikovite was reacted with citrate was necessary in order to achieve consistent steady state dissolved uranium concentrations at each flow rate, as shown in Fig. 4. Without the pretreatment, uranium concentrations increased rapidly, reached a peak and then slowly decreased, and the pattern was repeated at each flow rate with no consistency or discernible trends with citrate concentrations (Fig. S5). For all citrate concentrations, more than half of the total dissolved uranium over the course of the experiment was released during the pretreatment process indicating the existence of a readily soluble phase on the surface of the chernikovite (Table 2). The pretreatment step also helped to maintain a constant pH 4 throughout the experiments (Fig. S6). However, the 0.1 mM citrate experiment was an exception because the effluent pH reached 6 whenever citrate was present even though the influent solution maintained a pH of 4. Based on speciation calculations using Visual MINTEQ under these experimental conditions, this shift in pH should have minimal effect on the speciation of uranium and dissolution reactions.

After the pretreatment in systems with citrate present, the dissolved uranium concentration increased (Cervini-Silva et al., 2012; Edayilam et al., 2018) sharply, and then the rate of change diminished and approached a steady value (Fig. 4). This occurred during successive decreases in flow rate, leading to a step-like pattern in the time series where each flow rate results in a quasi-steady state uranium concentration for each citrate concentration. When the citrate concentration in the influent was increased, the uranium concentration in the effluent increased but retained the step-like pattern that occurred at each flow rate. The dissolved uranium concentrations for the experiment with no citrate in solution remained relatively constant despite the changing flow rate with an overall average of 6.83 ± 0.29 μM (Fig. 4).

The increase in dissolved uranium concentrations with decreasing flow rates was most prevalent in the 1 mM citrate experiment, where the decreases in the flow rate from 1 mL/min to 0.5 mL/min and then from 0.5 mL/min to 0.25 mL/min increased the steady state concentrations of

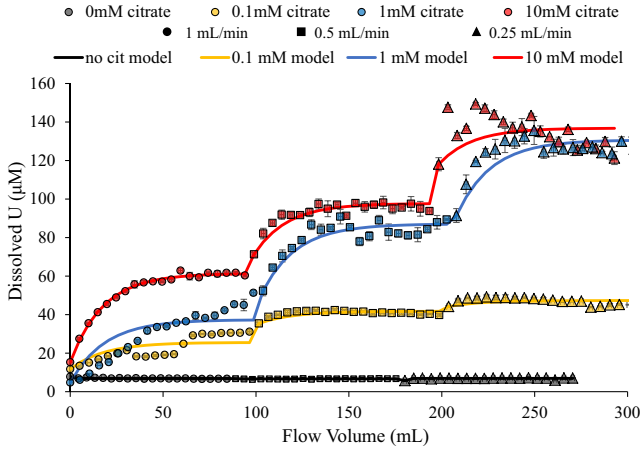


Fig. 4. Dissolution of chernikovite in a continuously stirred tank reactor with four different concentrations of citrate (denoted by marker color) and three different flow rates (denoted by marker shape) at pH 4. The error bars are the standard deviation in the analysis and are mostly smaller than the markers. The solid line represents the modeled concentrations. (For interpretation of the references to color in this figure legend, the reader is referred to the web version of this article.)

the dissolved uranium by a factor of 2.0 and 1.5 respectively. For the 10 mM citrate, the steady state concentration of the dissolved uranium increased by a factor of 1.6 as the flow rate decreased from 1 to 0.5 mL/min and by a factor of 1.3 as the flow rate decreased from 0.5 to 0.25 mL/min. The dissolved uranium concentrations from the 0.1 mM citrate experiment increased the least with the change in flow rates resulting in an increase in the steady state concentration by a factor of 1.4 for the first decrease in flow rate and 1.1 for the second.

The total amount of uranium dissolved in the absence of citrate is 4.64 μmol, whereas the total amount of uranium dissolved in the 10 mM citrate experiment is 88.6 μmol (27.7 μmol after pretreatment) (Table 2). The greatest dissolved uranium concentrations occurred at the 0.25 mL/min flow rate, and at steady state (after approximately 3 reactor volumes of flow after the flow rate was switched) they were 45.5 ± 1.2 μM for 0.1 mM citrate, 125.4 ± 3.5 μM for 1 mM citrate, and 128.8 ± 4.5 μM for 10 mM citrate (Fig. 4). Although the dissolved uranium concentrations increased overall with increasing citrate concentrations, the steady state dissolved uranium concentrations converged for the 1 mM and 10 mM citrate systems as flow rate decreased.

Although phosphate concentration was not measured throughout the dissolution experiment, the U:P ratio was determined for the remaining solid and solution at the end of each experiment. Both the solid and solution each had a 1:1 U:P ratio.

4. DISCUSSION

The results of the experiments provide several perspectives on the processes and extent to which citrate affects the dissolution of uranium. There are at least three relevant conceptual models outlining mechanisms to explain ligand-promoted dissolution: 1.) surface complexation; 2.) ligand surface saturation; and 3.) secondary-phase precipitation. Each of these mechanisms are briefly discussed as a series of multiple working hypotheses to provide context for evaluating the experimental data from the current work (Chamberlin, 1965).

4.1. Conceptual models of ligand-promoted dissolution

4.1.1. Surface complexation

Ligand-promoted dissolution is commonly viewed as a two-step process with one ligand complexing a cation within a mineral, which then promotes dissolution (Fig. 5A). However, when the counter anion in the mineral phase dissolves in parallel with the cation, competition between the two ligands may occur leading to a complex ternary system. This is exacerbated in the uranyl phosphate system examined in this work due to the potential formation of aqueous uranyl phosphate complexes that may lead to saturation and re-precipitation. In carbonate-enhanced dissolution, Gudavalli et al. (2013) propose that the ligand coordinates with uranyl polyhedrons at the mineral surface, and then the surface complex detaches to form aqueous uranyl-ligand complexes. The breaking of the uranyl-ligand complexes from the mineral surface is a rate-limiting second step. Reinoso-Maset et al. (2017) suggest the same process as a possible mechanism for the dissolution of uranyl oxyhydroxide mineral dissolution in a high carbonate system and hypothesize a relatively fast adsorption and desorption process due to an absence of evidence for an altered layer that could occur with prolonged uranyl-ligand surface complexes. This mechanism implies that uranium dissolution will increase with increasing citrate concentrations as long as uranyl phosphate mineral remains in the system.

4.1.2. Ligand surface saturation

An alternative mechanism includes the formation of an altered layer due to surface saturation. The citrate complexes with the uranyl polyhedron at the mineral surface, but excess citrate saturates the surface and hinders the release of the uranyl-citrate complexes into the aqueous

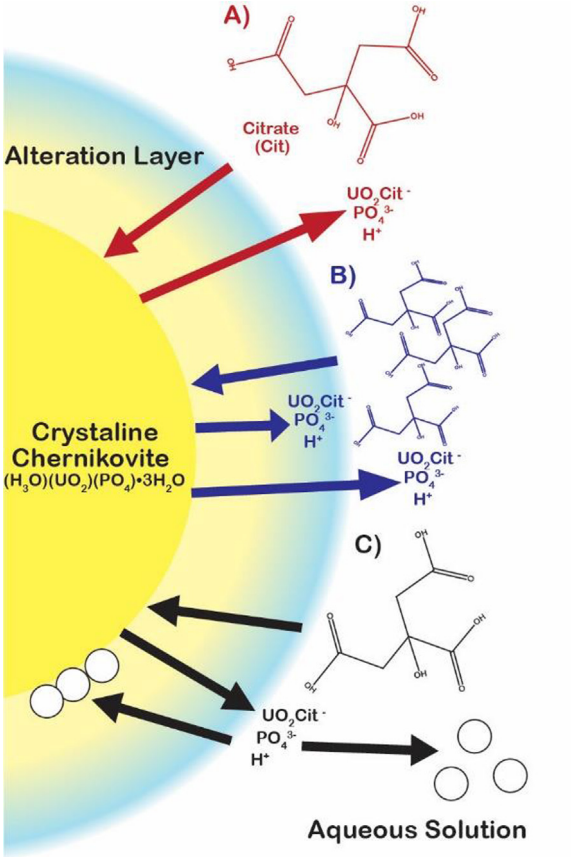


Fig. 5. Conceptual model of three potential mechanisms of citrate-promoted dissolution: (A) surface complexation where citrate complexes with uranyl at the mineral surface and then detaches from surface as uranyl-citrate aqueous complex, (B) ligand surface saturation where citrate complexes with uranyl at the mineral surface, but excess citrate saturates surface and hinders the release of uranyl-citrate into the aqueous solution, (C) secondary-phase precipitation where citrate complexes with uranyl at the mineral surface and uranyl-citrate is released into solution, but the dissolved uranium and dissolved phosphate reprecipitate as a secondary-phase mineral.

solution (Fig. 5B). Therefore, an alteration layer of uranyl-citrate complexes would accrue at the mineral surface. For this mechanism, uranium dissolution will increase with increasing citrate concentrations until the citrate concentrations are great enough to saturate the chernikovite surface at which point the dissolved uranium concentration will change little as citrate increases.

4.1.3. Secondary-phase precipitation

Another mechanism involves the recrystallization or formation of a secondary-phase mineral with the dissolved uranium and phosphate, which has been suggested in previous studies (Wellman et al., 2006, 2007; Gudavalli et al., 2013, 2018; Reinoso-Maset et al., 2020) (Fig. 5C). Similar to the first hypothesized mechanism, citrate complexes with the uranyl polyhedron forming a surface complex that is then released into the aqueous solution along with phosphate. However, the increasing aqueous uranium and citrate concentrations may lead to saturation and re-precipitation of uranyl phosphate due to the quick precipitation kinetics. This secondary precipitation could be a less soluble form of chernikovite or another uranyl phosphate mineral, both of which would be more thermodynamically favorable (e.g., less soluble). To support this secondary-phase precipitation mechanism hypothesis, uranium dissolution would increase with increasing citrate concentration until dissolved uranium and phosphate concentrations reach a saturation limit at which the uranium and phosphate will approach steady concentrations controlled by the new uranyl phosphate precipitates.

4.2. Effects of increasing citrate concentrations on the dissolution of uranium

If the simple, two-step, surface complexation mechanism shown in Fig. 5A is responsible for the citrate-promoted dissolution, then the uranium concentration is expected to change in proportion to the citrate concentration as long as uranium is available. Speciation analysis using Visual MINTEQ indicates that chernikovite solubility is increased through the formation of uranyl-citrate complexes. The batch dissolution experiments support that the dissolved uranium concentration consistently increase when equilibrated with citrate concentrations up to 10 mM. However, above 10 mM citrate, the change in dissolved uranium concentrations versus citrate concentration was much smaller. This smaller increase in dissolved uranium concentrations with increasing ligand concentrations suggests that the release of uranium is hindered at greater citrate concentrations. Thus, the simple two-step, surface complexation mechanism of chernikovite dissolution (Fig. 5A) is likely not occuring at high citrate concentrations. However, the data are consistent with the expected trends if ligand surface saturation or secondary-phase precipitation (Fig. 5B and Fig. 5C) govern citrate-promoted dissolution of chernikovite. With these mechanisms the dissolution of uranium is hindered at greater citrate concentrations.

The similar uranium aqueous concentrations observed at 12 h and one week indicate the dissolution step was not kinetically limited on the order of hours. In previous studies with immobile uranium phases and organic ligands, the uranium concentration reached steady state after several days (Wellman et al., 2006; Luo and Gu, 2011). The faster dissolution kinetics during this study could be due to the low pH used in this study and different uranium solid phases.

Comparisons of the experimental data and geochemical speciation modeling indicates that the chernikovite phase may be transient and slowly alter to Na-autunite with lower solubility or be able to re-crystallize given longer dissolution/reaction times. The prediction of only Na-autunite precipitation by the geochemical speciation modeling at the higher citrate concentrations shown in Fig. 1 is likely due to greater sodium concentrations coincident with greater citrate concentrations due to the use of sodium citrate dihydrate with a 3:1 sodium:citrate ratio. In their study, Reinoso-Maset et al. (2020) observed similar changes in the initial uranyl phosphate mineral compositions and

formation of new minerals due to cation exchange from exposure to simulated porewater.

Corroborating the results of the batch dissolution experiments, the citrate sorption experiments also suggest a quick initial reaction. The rapid adsorption of citrate and release of uranium indicates that the rate of citrate adsorption is not a limiting factor as discussed with respect to Fig. 2. The subsequent decrease in dissolved uranium concentration suggests the formation of a secondary-phase precipitate that would provide additional surfaces for citrate sorption resulting in the increased sorbed citrate concentrations. The formation of a secondary or more ordered phase will be dependent on the total mass of uranium leached into solution and thus, dependent on the total citrate concentration. Based on these observations and simulations which suggests a fast dissolution reaction, the batch tests were complimented using CSTR experiments in order to more precisely control the reaction times with respect to the approach to equilibrium.

For the experiments with citrate in the CSTR, the longer hydraulic residence times that occur with the lower flow rates provided a longer interaction time for the citrate and chernikovite, which resulted in greater dissolved uranium concentrations, creating the step-like pattern observed in Fig. 4. This continued increase in dissolved uranium concentrations with longer hydraulic residence times implies that although the reaction reaches a quasi-steady state at each flow rate, the systems with citrate have not reached an equilibrium within the 72-min hydraulic residence time at the slowest flow rate, (Fig. 4). However, in the experiment without citrate, the dissolved uranium concentrations remained relatively constant despite the changing flow rate. This constant concentration, even as the hydraulic residence time increased with the decreasing flow rate, suggests that the system without citrate has reached equilibrium. This equilibrium concentration of 6.83 $\pm$ 0.29 μM was used to calculate the K_{sp} of the synthesized chernikovite, and this uranium concentration is comparable to the 8.05 μM observed with the no citrate system in the batch solution after a week.

Although the increase in dissolved uranium concentration with decreasing flow rate is observed in all the CSTR experiments with citrate, the extent of this trend is dependent on the concentration of citrate in the solution. The 0.1 mM citrate experiment has the smallest increase between flow rates, particularly between the 0.5 mL/min and 0.25 mL/min flow rates (Fig. 4), which suggests that the system with 0.1 mM citrate may be approaching equilibrium and is similar to the no citrate system. As in the batch experiments, dissolved uranium concentration increases with increasing citrate concentration in the CSTR experiments. However, the dissolved uranium concentrations in the 1 mM and 10 mM converge as the flow rate decreases resembling the smaller increase in dissolved uranium concentrations observed at the higher citrate concentration in the batch experiments. The comparable uranium concentrations in the 1 mM and 10 mM CSTR systems at the 0.25 mL/min flow rate (Fig. 4) suggests that further uranium dissolution is hindered due to a combination of surface saturation of citrate at higher concentrations (Fig. 5B) and formation of a secondary-phase precipitate or more ordered uranyl phosphate phase (Fig. 5C). The potential re-precipitation or formation of a more ordered, less-soluble uranyl phosphate phase may be facilitated by the longer residence times, the increased sodium concentrations from the sodium citrate, and higher dissolved uranium and phosphate concentrations from citrate-promoted dissolution. Note that for the latter to transpire, dissociation of the uranyl-citrate aqueous complexes must occur, which is expected as the total dissolved uranium concentration increases and the total citrate concentration remains constant (e.g., a constant influent concentration of sodium citrate). Aqueous uranyl phosphate complexes may form in the system though the mineral phases are more critical for controlling dissolved uranium concentrations.

4.3. Evidence of secondary-phase precipitation

Although the chemical equilibrium model predicted the secondary-phase precipitation of uranyl orthophosphate (3:2 uranium to phosphorous ratio) at low citrate concentrations, both the solids and solutions remaining after exposure to 0.1 mM, 1 mM, and 10 mM citrate concentrations had a 1:1 U:P ratio. This consistency in the U:P ratio from the start and end of both the batch and CSTR experiments suggests that any re-precipitation was a Na-autunite or a more insoluble form of chernikovite. Although the similarity in the XRD patterns of the starting chernikovite and the post-experiment uranyl phosphate could suggest no change in the starting material (Fig. S1), the formation of Na-autunite as a secondary-phase precipitate is still a possibility because of the nearly identical diffraction patterns of chernikovite and Na-autunite. The molar increase in sodium in comparison to the moles of uranium and phosphorus revealed by the EDS analysis also indicates that a Na-autunite (1:1:1 Na to P to U ratio) may be forming as a secondary-phase precipitate in the presence of citrate. The lack of evidence for uranyl orthophosphate secondary-phase precipitation despite the favorable thermodynamics at low citrate concentrations agrees with previous work and suggests that uranyl orthophosphate is kinetically unfavorable in these conditions compared to chernikovite or Na-autunite (Mehta et al., 2014).

4.4. Evidence of ligand surface saturation effects

The peak shifts observed in the Raman spectra of the uranyl phosphate exposed to citrate corresponds to uranyl-citrate association on the remaining uranyl phosphate solid (Fig. 3). This change in the Raman spectra could be evidence of an alteration layer where citrate interacts with surface uranyl to the extent that it can be detected by Raman.

The comparison between the computed theoretical Raman spectra and the experimental Raman spectra suggest that citrate predominantly interacts with the surface uranyl in a 1:2 middle configuration. Other combinations may be present to a lesser extent. Although a 1:2 uranyl to citrate complex is favored at the chernikovite surface, speciation modelling revealed that the UO_2-citrate$^-$ was

the predominant aqueous uranyl complex under the experimental conditions.

These findings offer an alternative explanation for the nonlinear relationship between uranium and citrate concentrations discovered in the batch experiments in addition to secondary-phase precipitation. At high citrate concentrations the coordination of the citrate with a 1:2 uranyl to citrate ratio at the surface forms an alteration layer from saturating the surface with citrate. The citrate layer surrounding the surface could spatially hinder and limit the surface diffusion and mass transfer of the uranyl-citrate complex into an aqueous phase. The formation of an alteration layer composed of uranyl-citrate surface complexes suggests that the dissolution mechanism in Fig. 5B is favored over the rapid release of the uranyl-citrate surface complex needed for the mechanisms described in Fig. 5A. These findings are consistent with qualitative observations made when preparing samples for XRD and Raman analysis that the higher citrate concentrations result in a more uniform, homogenous particle size distribution indicating that the citrate is coating the surface and minimizing aggregation (Fig. S7).

4.5. Reaction rate of citrate-promoted dissolution of chernikovite

The CSTR data was best fit with a pseudo zero-order model that considers the dissolved uranium concentration over time (represented by flow rate divided by volume) relative to $[U]_{eq}$, the predicted concentration of dissolved uranium at equilibrium (Eq. (3); Fig. 4). The $[U]_{eq}$ was calculated using a log K_{sp} of −13.52 determined by the results of the no-citrate CSTR experiment and is slightly lower than the value of −13.17 reported by Gorman-Lewis et al. (2009). When the more negative log K_{sp} values reported for the more ordered (e.g., crystalline) chernikovite were used, the predicted dissolved uranium concentrations were less than the dissolved uranium concentrations observed during the experiment, which led to the assumption that the chernikovite used in this study is more amorphous.

An increase in the dissolution rate constants was observed with increasing citrate concentrations consistent with speciation calculations indicating more aqueous uranyl-citrate complexes will form and therefore increase solubility. With the addition of 0.1 mM citrate, the chernikovite dissolution rate constant increased by a factor 3.8 compared to the dissolution rate constant of a system without citrate. For the systems with citrate the dissolution rate constants increased in the order $2.39 \pm 0.12 \times 10^{-8}$ mol L s^{-1}, $3.49 \pm 0.17 \times 10^{-8}$ mol L s^{-1}, and $5.72 \pm 0.03 \times 10^{-8}$ mol L s^{-1} for 0.1 mM, 1 mM, and 10 mM citrate, respectively, when the flow rate was at 1 mL/min (Table 4 and Fig. 4). Based on these results, an increase in the citrate concentration by a factor of 10 increased the dissolution rate by a factor of approximately 1.5.

For the two slower flow rates, the increase in dissolution rates between the 1 mM citrate experiment and the 10 mM citrate experiment was less than the increase in rates between the 0.1 mM and 1 mM citrate experiments. At the slower flow rates, of 0.25 and 0.5 mL/min, the reaction products are being removed from the CSTR at a slower rate allowing the system to come closer to equilibrium where reverse reactions, such as the hypothesized secondary precipitation, may be impactful and influence the reaction constants k and n. Model fits for individual flow rate regimes at a constant citrate concentration yield rate constants that appear to trend towards slower rate constants as flow rate decreases. Though the trend is visible in Fig. 6, it is noteworthy that the fitted rate constants for each flow rate regime are not statistically significantly different (p value < 0.05). A second model applying one global reaction constant to each flow rate regime consistently underfit the 1.0 and 0.5 mL/min flow rate periods and overfit the 0.25 mL/min flow rate period, indicating that secondary precipitation may be impacting the data collected at a slower flow rate, particularly the 10 mM citrate concentration system where the uranium concentration increases with the initial change in flow rate and then decreases (Fig. S8). This change in rate constants is unexpected because the rate constants should remain constant if the same equilibrium state is being approached at each flow rate and the citrate concentration does not change. However, formation of a secondary precipitate appears to occur during the longer reactions times and higher dissolved uranium concentrations of the slower flow rate experiments, and thus, produces a modified equilibrium state. Therefore, the slight decrease in reaction rates with decreasing flow rate is proposed to be an artifact of the secondary-phase formation. Due to this artifact, the data from the 1 mL/min flow rate are the most appropriate for determination of the reaction constants.

The influence of citrate on chernikovite dissolution rates can be described adequately with a power law coefficient of approximately $n = 0.19 \pm 0.03$ and a log k' value of -6.8 ± 0.1 mol L^{-1} s^{-1} (Fig. 6). This expression can be used to correct the uranium dissolution rate constant in Eq. (3) for the influence of the total citrate concentration in the system. In previous work studying the effect of bicarbonate on the autunite dissolution rates, the regression analysis fits the data well and led to the prediction of the surface complexation conceptual model in Fig. 5A (Gudavalli et al., 2013). Therefore, the deviation in the regression analysis Eq. (4) at these higher citrate concentrations and slower flow rates suggests that the combined effects of surface saturation with citrate and the formation of a secondary-phase mineral hinder the release rate of uranium from chernikovite. However, these equations describe the change in dissolved uranium concentration only as a function of citrate concentration and further experiments are needed to elucidate the influence of other geochemical factors such as pH and the presence of competing ions like carbonate.

To account for specific surface interactions, a further study is needed to track the interaction of citrate, uranium, and phosphate at the surface interface of uranyl phosphate minerals. To develop a kinetic model that accurately includes a hinderance of the reaction rate due to citrate surface saturation/diffusion or secondary-phase precipitation, concentrations of uranium, phosphate, citrate, and sodium must be measured. The data could be further refined using a

Table 4
The chernikovite dissolution rate constants determined for each citrate concentration at the three flow rates tested where k is the rate constant used in the model and k^* is the reaction rate normalized by surface area.

Citrate Concentration	1 mL/min flow rate		0.5 mL/min flow rate		0.25 mL/min flow rate	
	k (mol L^{-1} s^{-1})	k* (mol m^{-2} s^{-1})	k (mol L^{-1} s^{-1})	k* (mol m^{-2} s^{-1})	k (mol L^{-1} s^{-1})	k* (mol m^{-2} s^{-1})
no citrate	$>6.23 \pm 0.04 \times 10^{-9}$	$>2.02 \pm 0.17 \times 10^{-9}$	–	–	–	–
0.1 mM	$2.39 \pm 0.11 \times 10^{-8}$	$4.07 \pm 0.19 \times 10^{-9}$	$1.95 \pm 0.02 \times 10^{-8}$	$3.36 \pm 0.15 \times 10^{-9}$	$1.10 \pm 0.01 \times 10^{-8}$	$1.94 \pm 0.09 \times 10^{-9}$
1 mM	$3.49 \pm 0.17 \times 10^{-8}$	$1.13 \pm 0.10 \times 10^{-8}$	$4.06 \pm 0.05 \times 10^{-8}$	$1.35 \pm 0.12 \times 10^{-8}$	$3.05 \pm 0.04 \times 10^{-8}$	$1.10 \pm 0.1 \times 10^{-8}$
10 mM	$5.72 \pm 0.02 \times 10^{-8}$	$1.22 \pm 0.07 \times 10^{-8}$	$4.55 \pm 0.04 \times 10^{-8}$	$1.01 \pm 0.06 \times 10^{-8}$	$3.19 \pm 0.07 \times 10^{-8}$	$7.48 \pm 0.46 \times 10^{-9}$

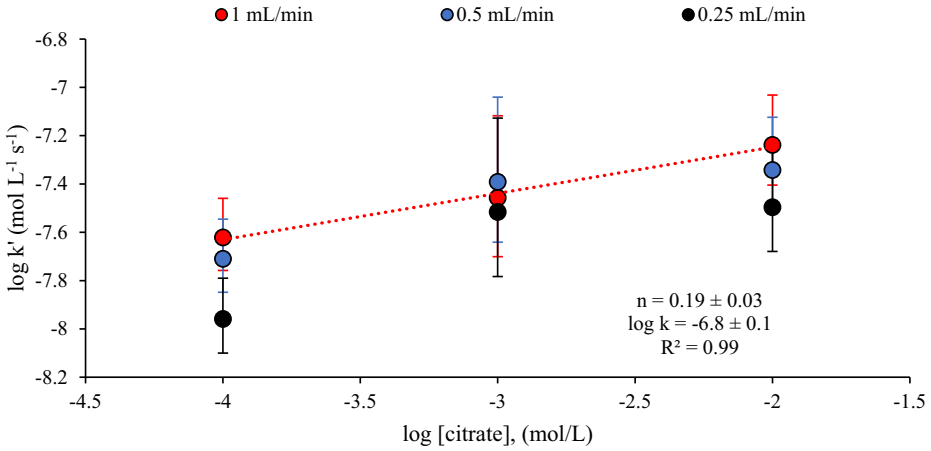


Fig. 6. The dissolution rate of uranium as a function of citrate solution concentration with 1 mL/min, 0.5 mL/min, and 0.25 mL/min flow rates. Uncertainties of the rate constants were determined using nonlinear regression in the program SAS.

more ordered form of chernikovite, which is not as likely to facilitate formation of secondary precipitates as proposed in this work.

4.6. Broader geochemical significance

On a broader scope, it is reasonable to assume the impacts of surface alteration and secondary precipitation will be observed in other mineral systems. The results from this work demonstrate the impact of secondary mineral precipitation occurring during ligand-promoted dissolution studies. Dissolution studies which involve metastable minerals, such as a more disordered phase or a kinetically limited phase, may transition from local thermodynamic minimums during the dissolution studies (*e.g.*, from less thermodynamically favorable to more thermodynamically favorable phases), as proposed in this work. Thus, the kinetic rate constants determined from such data would need to account for the changing thermodynamic endpoints, which profoundly complicates the data analysis as only limited information on transitions from such local minimums is available. These complications are particularly noteworthy in ligand-promoted dissolution studies where ligand surface saturation and/or formation of an alteration layer at the mineral surface may occur. Experiments designed to monitor all components of ternary dissolution systems and incorporate monitoring of surface ligand saturation/diffusion rates and secondary phase precipitation may yield the necessary data to parameterize a complex kinetic dissolution model where transformation from metastable states may be occurring.

5. CONCLUSIONS

The experiments described in this paper verify that citrate increases the dissolution rate of chernikovite by up to an order of magnitude with the increase in reaction rate dependent on the concentration of citrate. Overall, it is clear that citrate can enhance the dissolution of chernikovite, but the magnitude of increase is only weakly influenced by increasing citrate concentration with a reaction order of 0.19. This finding is supported by batch and CSTR dissolution, solid phase chernikovite characterization before and after exposure to citrate, and citrate sorption experiments, which provide insight into the specific interaction of citrate-promoted dissolution of chernikovite. A conceptual model based on these results indicates the possibility of an alteration layer on the chernikovite surface forming with citrate saturating the surface as well as a secondary-phase precipitation of a less soluble phase than the original. This indicates that the effects of ligands, like citrate-promoted dissolution should be considered in the

analysis of contaminated sites where uranyl phosphate controls the release of uranium, particularly in near surface environments where plant exudates (including citrate) can enhance uranium dissolution. A set of reaction rate constants has been determined in this work that can be used to determine the rate and extent of enhanced uranyl phosphate mineral dissolution. For a practical field application, the similarity in reaction rates determined at different flow rates implies the rates only from the 1 mL/min could be used or the rates could be averaged. However, the slight changes in reaction rate constants with flow rate in CSTR experiments highlights the potential impacts of secondary-phase formation that require further study in order to fully ascertain the impacts of these phases.

Declaration of Competing Interest

The authors declare that they have no known competing financial interests or personal relationships that could have appeared to influence the work reported in this paper.

ACKNOWLEDGMENT

This material is based upon work supported by the U.S. Department of Energy Office of Science, Office of Basic Energy Sciences and Office of Biological and Environmental Research under Award Number DE-SC-0012530.

APPENDIX A. SUPPLEMENTARY MATERIAL

Supplementary data to this article can be found online at https://doi.org/10.1016/j.gca.2021.11.023.

REFERENCES

Banfield J. F., Barker W. W., Welch S. A. and Taunton A. (1999) Biological impact on mineral dissolution: application of the lichen model to understanding mineral weathering in the rhyzosphere. *Procedings Natl. Acad. Sci.* **96**, 3404–3411.

Bar-Tal A., Feigenbaum S., Sparks D. L. and Pesek J. D. (1990) Analyses of Adsorption Kinetics Using a Stirred-Flow Chamber: I. Theory and Critical Tests. *Soil Sci. Soc. Am. J.* **54**, 1273.

Becke A. D. (1993) A new mixing of Hartree-Fock and local density-functional theories. *J. Chem. Phys.* **98**, 1372–1377.

Bostick B. C., Fendorf S., Barnett M. O., Jardine P. M. and Brooks S. C. (2002) Uranyl Surface Complexes Formed on Subsurface Media from DOE Facilities. *Soil Sci. Soc. Am. J.* **66**, 10.

Buck E. C., Brown N. R. and Dietz N. L. (1996) Contaminant Uranium Phases and Leaching at the Fernald Site in Ohio. *Environ. Sci. Technol.* **30**, 81–88.

Burns P. C. (2005) U6+ Minerals and inorganic compounds: Insights into an expanded structural hierarchy of crystal structures. *Can. Mineral.* **43**, 1839–1894.

Cervini-Silva J. (2005) Biogenic dissolution of a soil cerium-phosphate mineral. *Am. J. Sci.* **305**, 711–726.

Cervini-Silva J., Kearns J. and Banfield J. (2012) Steady-state dissolution kinetics of mineral ferric phosphate in the presence of desferrioxamine-B and oxalate ligands at pH=4–6 and T=24 ±0.6°C. *Chem. Geol.* **320–321**, 1–8.

Chamberlin T. C. (1965) The Method of Multiple Working Hypotheses. *Science* **148**, 754–759.

Clavier N., Crétaz F., Szenknect S., Mesbah A., Poinssot C., Descostes M. and Dacheux N. (2016) Vibrational spectroscopy of synthetic analogues of ankoleite, chernikovite and intermediate solid solution. *Spectrochim. Acta. A. Mol. Biomol. Spectrosc.* **156**, 143–150.

Craft E. S., Abu-Qare A. W., Flaherty M. M., Garofolo M. C., Rincavage H. L. and Abou-Donia M. B. (2004) Depleted and Natural Uranium: chemistry and Toxicological effects. *J. Toxicol. Environ. Health Part B* **7**, 297–317.

Driscoll R. J. P., Wolverson D., Mitchels J. M., Skelton J. M., Parker S. C., Molinari M., Khan I., Geeson D. and Allen G. C. (2014) A Raman spectroscopic study of uranyl minerals from Cornwall, UK. *RSC Adv.* **4**, 59137–59149.

Ebbs S. D., Brady D. J. and Kochian L. V. (1998) Role of uranium speciation in the uptake and translocation of uranium by plants. *J. Exp. Biol.* **49**, 1183–1190.

Edayilam N., Montgomery D., Ferguson B., Maroli A. S., Martinez N., Powell B. A. and Tharayil N. (2018) Phosphorus stress-induced changes in plant root exudation could potentially facilitate uranium mobilization from stable mineral forms. *Environ. Sci. Tech.* **52**, 7652–7662.

Fanizza M. F., Yoon H., Zhang C., Oostrom M., Wietsma T. W., Hess N. J., Bowden M. E., Strathmann T. J., Finneran K. T. and Werth C. J. (2013) Pore-scale evaluation of uranyl phosphate precipitation in a model groundwater system. *Water Resour. Res.* **49**, 874–890.

Francis A. J. and Dodge C. J. (1998) Remediation of soils and wastes contaminated with uranium and toxic metals. *Environ. Sci. Technol.* **32**, 3993–3998.

Fuller C. C., Bargar J. R., Davis J. A. and Piana M. J. (2002) Mechanisms of uranium interactions with hydroxyapatite: implications for groundwater remediation. *Environ. Sci. Technol.* **36**, 158–165.

Gao N., Huang Z., Liu H., Hou J. and Liu X. (2019) Advances on the toxicity of uranium to different organisms. *Chemosphere* **237** 124548.

Giammar D. (2001) Geochemistry of uranium at mineral-water interfaces: Rates of sorption-desorption and dissolution-precipitation reactions Dissertation (Ph.D.). California Institute of Technology.

Gorman-Lewis D., Burns P. C. and Fein J. B. (2008) Review of uranyl mineral solubility measurements. *J. Chem. Thermodyn.* **40**, 335–352.

Gorman-Lewis D., Shvareva T., Kubatko K.-A., Burns P. C., Wellman D. M., McNamara B., Szymanowski J. E. S., Navrotsky A. and Fein J. B. (2009) Thermodynamic properties of autunite, uranyl hydrogen phosphate, and uranyl orthophosphate from solubility and calorimetric measurements. *Environ. Sci. Technol.* **43**, 7416–7422.

Grenthe I., Drozdizynski J., Fujino T., Buck E. C., Albrecht-Schmitt T. E. and Wolf S. F. (2011) Uranium. In *The Chemistry of the Actinide and Transactinide Elements* (eds. L. R. Morss, N. M. Edelstein and J. Fuger). Springer, Dordrecht, Netherlands, pp. 253–698.

Gudavalli R. K. P., Katsenovich Y. P., Wellman D. M., Idarraga M., Lagos L. E. and Tansel B. (2013) Comparison of the kinetic rate law parameters for the dissolution of natural and synthetic autunite in the presence of aqueous bicarbonate ions. *Chem. Geol.* **351**, 299–309.

Gudavalli R., Katsenovich Y. and Wellman D. (2018) Quantification of kinetic rate law parameters for the dissolution of natural autunite in the presence of aqueous bicarbonate ions at high concentrations. *J. Environ. Radioact.* **190–191**, 1–9.

Huang J. W., Blaylock M. J., Kapulnik Y. and Ensley B. D. (1998) Phytoremediation of uranium-contaminated soils: role of

organic acids in triggering uranium hyperaccumulation in plants. *Environ. Sci. Technol.* **32**, 2004–2008.

Küchle W., Dolg M., Stoll H. and Preuss H. (1994) Energy-adjusted pseudopotentials for the actinides. Parameter sets and test calculations for thorium and thorium monoxide. *J. Chem. Phys.* **100**, 7535–7542.

Lee C., Yang W. and Parr R. G. (1988) Development of the Colle-Salvetti correlation-energy formula into a functional of the electron density. *Phys. Rev. B* **37**, 785–789.

Liu C., Zachara J. M., Zhong L., Kukkadupa R., Szecsody J. E. and Kennedy D. W. (2005) Influence of sediment bioreduction and reoxidation on uranium sorption. *Environ. Sci. Technol.* **39**, 4125–4133.

Luo W. and Gu B. (2011) Dissolution of uranium-bearing minerals and mobilization of uranium by organic ligands in a biologically reduced sediment. *Environ. Sci. Technol.* **45**, 2994–2999.

McGrail B. P., Elbert W. L., Bakel A. J. and Peeler D. K. (1997) Measurement of kinetic rate law parameters on a Na-Ca-Al borosilicate glass for low-activity waste. *J. Nucl. Mater.* **249**, 175–189.

Mehta V. S., Maillot F., Wang Z., Catalano J. G. and Giammar D. E. (2014) Effect of co-solutes on the products and solubility of uranium(VI) precipitated with phosphate. *Chem. Geol.* **364**, 66–75.

Mehta V. S., Maillot F., Wang Z., Catalano J. G. and Giammar D. E. (2015) Transport of U(VI) through sediments amended with phosphate to induce in situ uranium immobilization. *Water Res.* **69**, 307–317.

Moon H. S., Komlos J. and Jaffé P. R. (2007) Uranium reoxidation in previously bioreduced sediment by dissolved oxygen and nitrate. *Environ. Sci. Technol.* **41**, 4587–4592.

Murakami T., Ohnuki T., Isobe H. and Sato T. (1997) Mobitity of uranium during weathering. *Am. Mineral.* **82**, 888–899.

Palmisano A. and Hazen T. (2003) Bioremediation of metals and radionuclides: what it is and how it works (2nd edition). United States.

Perdrial N., Vázquez-Ortega A., Wang G., Kanematsu M., Mueller K. T., Um W., Steefel C. I., O'Day P. A. and Chorover J. (2018) Uranium speciation in acid waste-weathered sediments: the role of aging and phosphate amendments. *Appl. Geochem.* **89**, 109–120.

Reinoso-Maset E., Perdrial N., Steefel C. I., Um W., Chorover J. and O'Day P. A. (2020) Dissolved carbonate and pH control the dissolution of uranyl phosphate minerals in flow-through porous media. *Environ. Sci. Technol.* **54**, 6031–6042.

Reinoso-Maset E., Steefel C. I., Um W., Chorover J. and O'Day P. A. (2017) Rates and mechanisms of uranyl oxyhydroxide mineral dissolution. *Geochim. Cosmochim. Acta* **207**, 298–321.

Riley R. G., Zachara J. M. and Wobber F. G. (1992) Chemical contaminant on DOE lands and selection of contaminant mixtures for subsurface science research. U.S Dept. of Energy, Office of Energy Research, Washington D.C..

Sani R. K., Peyton B. M., Dohnalkova A. and Amonette J. E. (2005) Reoxidation of reduced uranium with iron(III) (hydr) oxides under sulfate-reducing conditions. *Environ. Sci. Technol.* **39**, 2059–2066.

Seyfried M. S., Sparks D. L., Bar-Tal A. and Feigenbaum S. (1989) Kinetics of calcium magnesium exchange on soil using a stirred-flow reaction chamber. *Soil Sci. Soc. Am. J.* **53**, 406–410.

Shahandeh H. and Hossner L. R. (2002) Enhancement of uranium phytoaccumulation from contaminated soils. *Soil Sci.* **167**, 269–280.

Sowder A. G., Clark S. B. and Fjeld R. A. (2001) The impact of mineralogy in the U(VI)–Ca–PO4 system on the environmental availability of uranium. *J. Radioanal. Nucl. Chem.* **248**, 517–524.

Sparks D. L. (1989) Application of Chemical Kinetics to Soil Chemical Reactions. *Kinetics of Soil Chemical Processes*. Academic Press.

TURBOMOLE V6.4 2012, A development of University of Karlsruhe and Forschungszentrum Karlsruhe GmbH, 1989-2007, TURBOMOLE GmbH, since 2007; available from http://www.turbomole.com.

Ulrich K.-U., Ilton E. S., Veeramani H., Sharp J. O., Bernier-Latmani R., Schofield E. J., Bargar J. R. and Giammar D. E. (2009) Comparative dissolution kinetics of biogenic and chemogenic uraninite under oxidizing conditions in the presence of carbonate. *Geochim. Cosmochim. Acta* **73**, 6065–6083.

Ulrich K.-U., Singh A., Schofield E. J., Bargar J. R., Veeramani H., Sharp J. O., Bernier-Latmani R. and Giammar D. E. (2008) Dissolution of biogenic and synthetic UO_2 under varied reducing conditions. *Environ. Sci. Technol.* **42**, 5600–5606.

Van Haverbeke L. (1996) Solubility and spectrochemical characteristics of synthetic chernikovite and meta-ankoleite. *Mineral. Mag.* **60**, 759–766.

Veselý V., Pekárek V. and Abbrent M. (1965) A study on uranyl phosphates—III solubility products of uranyl hydrogen phosphate, uranyl orthophosphate and some alkali uranyl phosphates. *J. Inorg. Nucl. Chem.* **27**, 1159–1166.

Wang G., Um W., Wang Z., Reinoso-Maset E., Washton N. M., Mueller K. T., Perdrial N., O'Day P. A. and Chorover J. (2017) Uranium release from acidic weathered Hanford sediments: single-pass flow-through and column experiments. *Environ. Sci. Technol.* **51**, 11011–11019.

Welch S. A., Barker W. W. and Banfield J. F. (1999) Microbial extracellular polysaccharides and plagioclase dissolution. *Geochim. Cosmochim. Acta* **63**, 1405–1419.

Wellman D. M., Gunderson K. M., Icenhower J. P. and Forrester S. W. (2007) Dissolution kinetics of synthetic and natural meta-autunite minerals, $X_{3-n}^{(n\ )+}\ [(UO_2)(PO_4)]_2{\cdot}xH_2O$, under acidic conditions. *Geochem. Geophys. Geosyst.* **8**, n/a-n/a.

Wellman D. M., Icenhower J. P., Gamerdinger A. P. and Forrester S. W. (2006) Effects of pH, temperature, and aqueous organic material on the dissolution kinetics of meta-autunite minerals, $(Na,\ Ca)_{2-1}\ [(UO_2)(PO_4)]_2{\cdot}3H_2O$. *Am. Mineral.* **91**, 143–158.

Wu W.-M., Carley J., Luo J., Ginder-Vogel M. A., Cardenas E., Leigh M. B., Hwang C., Kelly S. D., Ruan C., Wu L., Van Nostrand J., Gentry T., Lowe K., Carroll S., Luo W., Fields M. W., Gu B., Watson D., Kemner K. M., Marsh T., Tiedje J., Zhou J., Fendorf S., Kitanidis P. K., Jardine P. M. and Criddle C. S. (2007) In situ bioreduction of uranium (VI) to submicromolar levels and reoxidation by dissolved oxygen. *Environ. Sci. Technol.* **41**, 5716–5723.

Associate editor: Carl Steefel